Numerical solution of a contact problem with unilateral constraint and history-dependent penetration

Mikael Barboteu · Weimin Han · Mircea Sofonea

Abstract A numerical method is presented for a mathematical model which describes the frictionless contact between a viscoplastic body and an obstacle, the so-called foundation. The process is quasistatic, and the contact is modeled with normal compliance and unilateral constraint, in such a way that the stiffness coefficient depends on the history of the penetration. A solution algorithm is discussed and implemented. Numerical simulation results are reported, illustrating the mechanical behavior related to the contact condition.

Keywords Augmented Lagrangian method · Finite element scheme · History-dependent stiffness coefficient · Normal compliance · Numerical simulations · Unilateral constraint

1 Introduction

Contact phenomena involving deformable bodies lead to nonsmooth, nonlinear mathematical problems. Analysis of the problems, including existence and uniqueness results, is carried out in a large number of works, see for instance [1–4] and the references therein. Numerical analysis of the problems, including error estimation for discrete schemes and numerical simulations, can be found in [5–9]. The state-of-the-art in the field, including applications in engineering, could be found in the recent special issue [10].

In this paper, we provide the numerical solution of a frictionless contact problem for viscoplastic materials. It models the quasistatic contact of a body with an obstacle made of a hard material covered with a thin layer of soft material, in the framework of the small deformation theory. The challenging feature of the problem is mainly caused by the forms of the constitutive law and the boundary condition on the contact surface. We describe the constitutive law of the material by a rate-type relation of the form

$$\dot{\boldsymbol{\sigma}} = \mathcal{E}\boldsymbol{\varepsilon}(\dot{\boldsymbol{u}}) + \mathcal{G}(\boldsymbol{\sigma}, \boldsymbol{\varepsilon}(\boldsymbol{u})), \tag{1.1}$$

M. Barboteu · M. Sofonea
Laboratoire de Mathématiques et Physique, Université de Perpignan Via Domitia, 52 Avenue Paul Alduy, 66860 Perpignan, France

W. Han (✉)
Department of Mathematics, University of Iowa, Iowa City, IA 52242, USA
e-mail: weimin-han@uiowa.edu

known as a viscoplastic constitutive law. Here, $\boldsymbol{u}$ represents the displacement vector, $\boldsymbol{\sigma}$ denotes the stress tensor, and $\boldsymbol{\varepsilon}(\boldsymbol{u})$ is the linearized strain tensor. The symbols $\mathcal{E}$ and $\mathcal{G}$ represent an elasticity tensor and a viscoplastic constitutive function, respectively. The dot above a variable represents the derivative of that variable with respect to the time, i.e., $\dot{f} = \partial f/\partial t$. Constitutive laws of the form (1.1) have been used in various papers in order to model the properties of real materials like metals, rocks, soils, and various polymers. Examples and mechanical interpretations can be found in [11,12] and the references therein. For the contact, we assume it is frictionless and is modeled with normal compliance and unilateral constraint. This condition was introduced in [13] and then used in a large number of papers, see the references in [14]. Unlike the Signorini condition which expresses the requirement of nondeformability of the obstacle, the normal compliance condition with unilateral constraint allows the penetration of the obstacle. The latter is described by a surface property parameter, the stiffness coefficient. The novelty of the model we consider in this paper is that the stiffness coefficient is allowed to depend on the history of the penetration.

Analysis of various quasistatic frictionless and frictional contact problems for such kind of materials was carried out in various works, see for instance [2,4,15–18]. The book [2] deals with both the variational and numerical analyses of the problems; there, existence and uniqueness results are presented, semi-discrete and fully discrete schemes for various contact models are studied, error estimates are obtained, and convergence results are proved. The book [4] describes various contact models and their variational formulations. It also provides unique solvability results and representative proofs. For the problem considered in [17], the contact is described with the Signorini condition in a form with a zero gap function; there, an evolutionary mixed variational formulation of the corresponding contact problem is derived, and the unique solvability of the model is shown by using arguments on saddle points theory, Lagrange multipliers, and fixed point. In contrast, in the papers [15,16], the contact is modeled with normal compliance and unilateral constraint. There, various existence, uniqueness, and convergence results are obtained, by using different functional methods. Also, numerical results are reported on two-dimensional test problems. The contact model in [15,16] was extended in [18], by considering the case when the stiffness coefficient depends on the history of the penetration. There, variational analysis of the problem, including its unique weak solvability, is provided. The proof is based on arguments of history-dependent variational inequalities.

The current paper is devoted to the numerical solution of the contact model introduced in [18] and is structured as follows. In Sect. 2, we first describe the mechanical problem together with the physical motivation which lead to this contact model, and then we list the assumptions on the data, state the variational formulation of the problem, and recall the existence and uniqueness result obtained in [18]. We complete it by recalling a particular case of the convergence result obtained in [18], which expresses the continuous dependence of the solution with respect to the stiffness coefficient. In Sect. 3, we describe the numerical method used to solve the problem, including details on a related hybrid variational formulation. In Sect. 4, we present numerical simulation results on a model two-dimensional problem, illustrating the mechanical behavior related to the contact condition, including the convergence result in Sect. 2. Some concluding remarks are given in Sect. 5.

2 The model

In this section, we present the mathematical model of contact we are interested in, together with some results in its analysis, obtained in [18].

The physical setting is the following. A viscoplastic body occupies, in its reference configuration, a bounded domain $\Omega \subset \mathbb{R}^d$ ($d = 2, 3$). The boundary $\partial\Omega = \Gamma$ of Ω is assumed to be Lipschitz continuous. We denote by $\boldsymbol{\nu} = (\nu_i)$ the unit outward normal, defined almost everywhere on Γ, and by $\boldsymbol{x} = (x_i)$ a typical point in $\Omega \cup \Gamma$. Here and below, the indices i, j, k, and l run between 1 and d, and unless stated otherwise, the summation convention over repeated indices is used. We use the symbol $\mathbb{S}^d$ for the space of second-order symmetric tensors on $\mathbb{R}^d$; the inner products and norms on $\mathbb{R}^d$ and $\mathbb{S}^d$ are defined by

$$\boldsymbol{u} \cdot \boldsymbol{v} = u_i v_i, \qquad \|\boldsymbol{v}\| = (\boldsymbol{v} \cdot \boldsymbol{v})^{1/2} \qquad \forall \boldsymbol{u}, \boldsymbol{v} \in \mathbb{R}^d,$$
$$\boldsymbol{\sigma} \cdot \boldsymbol{\tau} = \sigma_{ij}\tau_{ij}, \qquad \|\boldsymbol{\tau}\| = (\boldsymbol{\tau} \cdot \boldsymbol{\tau})^{1/2} \qquad \forall \boldsymbol{\sigma}, \boldsymbol{\tau} \in \mathbb{S}^d.$$

The boundary Γ is partitioned into three disjoint measurable parts Γ_1, Γ_2, and Γ_3, such that $meas\,(\Gamma_1) > 0$, and we denote that $[0, T]$ be the time interval of interest with some $T > 0$. The body is clamped on $\Gamma_1 \times (0, T)$, is submitted to the action of body forces, and surface tractions on $\Omega \times (0, T)$ and $\Gamma_2 \times (0, T)$, respectively, and is in contact with a deformable foundation on $\Gamma_3 \times (0, T)$. As a result, its mechanical state evolves, and the evolution is governed by the following mathematical model.

Problem $\mathcal{P}$ Find a displacement field $\boldsymbol{u} : \Omega \times [0, T] \to \mathbb{R}^d$ and a stress field $\boldsymbol{\sigma} : \Omega \times [0, T] \to \mathbb{S}^d$ such that

$$\dot{\boldsymbol{\sigma}} = \mathcal{E}\boldsymbol{\varepsilon}(\dot{\boldsymbol{u}}) + \mathcal{G}(\boldsymbol{\sigma}, \boldsymbol{\varepsilon}(\boldsymbol{u})) \quad \text{in } \Omega \times (0, T), \tag{2.1}$$

$$\mathrm{Div}\,\boldsymbol{\sigma} + \boldsymbol{f}_0 = \boldsymbol{0} \quad \text{in } \Omega \times (0, T), \tag{2.2}$$

$$\boldsymbol{u} = \boldsymbol{0} \quad \text{on } \Gamma_1 \times (0, T), \tag{2.3}$$

$$\boldsymbol{\sigma}\boldsymbol{\nu} = \boldsymbol{f}_2 \quad \text{on } \Gamma_2 \times (0, T), \tag{2.4}$$

$$\left.\begin{array}{l} u_\nu \le g,\ \sigma_\nu + K(\xi(u_\nu))p(u_\nu) \le 0, \\ (u_\nu - g)(\sigma_\nu + K(\xi(u_\nu))p(u_\nu)) = 0 \end{array}\right\} \quad \text{on } \Gamma_3 \times (0, T), \tag{2.5}$$

$$\boldsymbol{\sigma}_\tau = \boldsymbol{0} \quad \text{on } \Gamma_3 \times (0, T), \tag{2.6}$$

$$\boldsymbol{u}(0) = \boldsymbol{u}_0,\ \boldsymbol{\sigma}(0) = \boldsymbol{\sigma}_0 \quad \text{in } \Omega. \tag{2.7}$$

Let us comment on the equations and boundary conditions in (2.1)–(2.7) in which, for simplicity, we do not indicate explicitly the dependence of various functions on the variables $\boldsymbol{x}$ or t. Also, here and below we use the index ν and τ to denote the normal and tangential components of vectors and tensors, respectively.

Equation (2.1) represents the viscoplastic constitutive law of the material, already introduced in Sect. 1. Equation (2.2) is the equilibrium equation in which $\boldsymbol{f}_0$ represents the density of body forces; we use it here since the process is assumed to be quasistatic. In (2.1)–(2.2) and below, $\boldsymbol{\varepsilon}$ and Div are the deformation and the divergence operators, respectively, defined by

$$\boldsymbol{\varepsilon}(\boldsymbol{u}) = (\varepsilon_{ij}(\boldsymbol{u})), \quad \varepsilon_{ij}(\boldsymbol{u}) = \frac{1}{2}(u_{i,j} + u_{j,i}), \quad \mathrm{Div}\,\boldsymbol{\sigma} = (\sigma_{ij,j}),$$

where an index that follows a comma represents the partial derivative with respect to the corresponding component of the spatial variable, e.g., $u_{i,j} = \partial u_i / \partial x_j$. Conditions (2.3) and (2.4) are the displacement and traction boundary conditions, respectively, with $\boldsymbol{f}_2$ being the density of surface tractions. Condition (2.6) shows that the tangential stress on the contact surface vanishes, corresponding to a frictionless contact. In (2.7), $\boldsymbol{u}_0$ and $\boldsymbol{\sigma}_0$ are the initial displacement and the initial stress field, respectively.

We turn to the contact condition (2.5). First, the penetration is limited by a maximal depth $g > 0$. In other words, at any time t, the normal displacement on the contact surface $u_\nu(t)$ satisfies the inequality:

$$u_\nu(t) \le g. \tag{2.8}$$

Next, we assume that the normal stress has an additive decomposition of the form:

$$\sigma_\nu(t) = \sigma_\nu^D(t) + \sigma_\nu^R(t). \tag{2.9}$$

The part $\sigma_\nu^D(t)$ satisfies a normal compliance contact condition:

$$-\sigma_\nu^D(t) = Kp(u_\nu(t)). \tag{2.10}$$

Here p is a given nonnegative function which vanishes for negative arguments, and K represents the stiffness coefficient of the foundation. The normal compliance contact condition was used in many publications, see, e.g., [19–22] and references therein. The part $\sigma_\nu^R(t)$ of the normal stress satisfies the Signorini unilateral condition:

$$\sigma_\nu^R(t) \le 0, \quad \sigma_\nu^R(t)(u_\nu(t) - g) = 0. \tag{2.11}$$

We combine (2.9) and (2.10) to see that

$$\sigma_\nu^R(t) = \sigma_\nu(t) + Kp(u_\nu(t)). \tag{2.12}$$

Then, we substitute equality (2.12) in (2.11) and use (2.8), to obtain the condition:

$$u_\nu(t) \le g, \quad \sigma_\nu(t) + Kp(u_\nu(t)) \le 0, \quad (u_\nu(t) - g)\big(\sigma_\nu(t) + Kp(u_\nu(t))\big) = 0. \tag{2.13}$$

This condition can be naturally interpreted as follows: the foundation is made of a hard material covered by a thin layer of a softer material with thickness g; the soft material has an elastic behavior, i.e., it is deformable and allows penetration; the contact with this layer is modeled with normal compliance; the hard material is perfectly rigid, and, therefore, it does not allow penetration; the contact with this material is modeled using the Signorini contact condition. To conclude, condition (2.13) models a foundation which has a rigid-elastic behavior: its elastic behavior is given by the layer of the soft material, while its rigid behavior is given by the hard material.

Now, consider the more complicated situation where the stiffness coefficient can depend on the accumulation of penetration, denoted as $\xi(u_\nu)$:

$$K = K(\xi(u_\nu)(t)), \tag{2.14}$$

where

$$\xi(u_\nu)(t) = \int_0^t u_\nu^+(s)\, ds, \quad t \in [0, T], \tag{2.15}$$

where u_ν^+ is the positive part of u_ν. Combining (2.13) and (2.14) leads to the contact condition (2.5). Note that the dependence $K = K(\xi(u_\nu)(t))$ allows us to take into account the variation of the elastic modulus of the thin layer, as the cycles of contact and separation proceed and, therefore, it models the hardening or softening phenomenon. Practical examples of surface hardening or softening abound in industry and various engineering settings, see, e.g., [23].

To proceed with a variational formulation of the contact problem $\mathcal{P}$, we need some function spaces. We use the standard notation for Sobolev and Lebesgue spaces associated to Ω and Γ. In addition, let

$$V = \big\{\boldsymbol{u} = (u_i) :\ u_i \in H^1(\Omega), \quad u_i = 0 \ \text{ a.e. on } \Gamma_1\big\},$$
$$Q = \big\{\boldsymbol{\sigma} = (\sigma_{ij}) :\ \sigma_{ij} = \sigma_{ji} \in L^2(\Omega)\big\},$$
$$Q_1 = \big\{\boldsymbol{\sigma} \in Q :\ \mathrm{Div}\,\boldsymbol{\sigma} \in L^2(\Omega)^d\big\}.$$

These are real Hilbert spaces endowed with the canonical inner products:

$$(\boldsymbol{u}, \boldsymbol{v})_V = \int_\Omega \boldsymbol{\varepsilon}(\boldsymbol{u}) \cdot \boldsymbol{\varepsilon}(\boldsymbol{v})\, \mathrm{d}x,$$
$$(\boldsymbol{\sigma}, \boldsymbol{\tau})_Q = \int_\Omega \boldsymbol{\sigma} \cdot \boldsymbol{\tau}\, \mathrm{d}x,$$
$$(\boldsymbol{\sigma}, \boldsymbol{\tau})_{Q_1} = \int_\Omega \boldsymbol{\sigma} \cdot \boldsymbol{\tau}\, \mathrm{d}x + \int_\Omega \mathrm{Div}\boldsymbol{\sigma} \cdot \mathrm{Div}\, \boldsymbol{\tau}\, \mathrm{d}x.$$

The associated norms on these spaces are denoted by $\|\cdot\|_V$, $\|\cdot\|_Q$, and $\|\cdot\|_{Q_1}$, respectively. Recall that completeness of the space $(V, \|\cdot\|_V)$ follows from the assumption $\mathrm{meas}(\Gamma_1) > 0$, which allows the use of Korn's inequality. For an element $\boldsymbol{v} \in V$, we still write $\boldsymbol{v}$ for the trace of $\boldsymbol{v}$, and we denote by v_ν and $\boldsymbol{v}_\tau$ the normal and tangential components of $\boldsymbol{v}$, respectively, on Γ given by $v_\nu = \boldsymbol{v} \cdot \boldsymbol{\nu}$, $\boldsymbol{v}_\tau = \boldsymbol{v} - v_\nu \boldsymbol{\nu}$. Also, for a regular stress function $\boldsymbol{\sigma}$, we use the notations σ_ν and $\boldsymbol{\sigma}_\tau$, respectively, for the normal and the tangential traces, i.e., $\sigma_\nu = (\boldsymbol{\sigma}\boldsymbol{\nu}) \cdot \boldsymbol{\nu}$ and $\boldsymbol{\sigma}_\tau = \boldsymbol{\sigma}\boldsymbol{\nu} - \sigma_\nu \boldsymbol{\nu}$.

For every Banach space $(X, \|\cdot\|_X)$, we use the notation $C([0,T];X)$ for the space of continuous functions defined on $[0,T]$ with values on X. It is known that $C([0,T];X)$ is a real Banach space with the norm:

$$\|v\|_{C([0,T];X)} = \max_{t\in[0,T]} \|v(t)\|_X.$$

Moreover, for a subset $K \subset X$, we still use the symbol $C([0,T];K)$ for the set of continuous functions defined on $[0,T]$ with values in K.

In the study of the mechanical problem (2.1)–(2.7), we assume that the elasticity tensor $\mathcal{E}$, the constitutive function $\mathcal{G}$, the stiffness coefficient function K, and the normal compliance function p satisfy the following conditions:

$$\begin{cases} \text{(a) } \mathcal{E} = (\mathcal{E}_{ijkl}) : \Omega \times \mathbb{S}^d \to \mathbb{S}^d. \\ \text{(b) } \mathcal{E}_{ijkl} = \mathcal{E}_{klij} = \mathcal{E}_{jikl} \in L^\infty(\Omega),\ 1 \le i,j,k,l \le d. \\ \text{(c) There exists } m_{\mathcal{E}} > 0 \text{ such that } \mathcal{E}\boldsymbol{\tau}\cdot\boldsymbol{\tau} \ge m_{\mathcal{E}}\|\boldsymbol{\tau}\|^2 \text{ for all } \boldsymbol{\tau} \in \mathbb{S}^d, \text{ a.e. in } \Omega. \end{cases} \tag{2.16}$$

$$\begin{cases} \text{(a) } \mathcal{G} : \Omega \times \mathbb{S}^d \times \mathbb{S}^d \to \mathbb{S}^d. \\ \text{(b) There exists } L_{\mathcal{G}} > 0 \text{ such that } \|\mathcal{G}(\boldsymbol{x},\boldsymbol{\sigma}_1,\varepsilon_1) - \mathcal{G}(\boldsymbol{x},\boldsymbol{\sigma}_2,\varepsilon_2)\| \le L_{\mathcal{G}}\left(\|\boldsymbol{\sigma}_1-\boldsymbol{\sigma}_2\| + \|\varepsilon_1-\varepsilon_2\|\right) \\ \qquad \text{for all } \boldsymbol{\sigma}_1,\boldsymbol{\sigma}_2,\varepsilon_1,\varepsilon_2 \in \mathbb{S}^d, \text{ a.e. } \boldsymbol{x} \in \Omega. \\ \text{(c) The mapping } \boldsymbol{x} \mapsto \mathcal{G}(\boldsymbol{x},\boldsymbol{\sigma},\varepsilon) \text{ is measurable on } \Omega, \text{ for all } \boldsymbol{\sigma},\varepsilon \in \mathbb{S}^d. \\ \text{(d) The mapping } \boldsymbol{x} \mapsto \mathcal{G}(\boldsymbol{x},\mathbf{0},\mathbf{0}) \text{ belongs to } Q. \end{cases} \tag{2.17}$$

$$\begin{cases} \text{(a) } K : \Gamma_3 \times \mathbb{R}_+ \to \mathbb{R}_+. \\ \text{(b) There exists } L_K > 0 \text{ such that } |K(\boldsymbol{x},r_1) - K(\boldsymbol{x},r_2)| \le L_K|r_1-r_2| \\ \qquad \text{for all } r_1,\ r_2 \in \mathbb{R}_+, \text{ a.e. } \boldsymbol{x} \in \Gamma_3. \\ \text{(c) The mapping } \boldsymbol{x} \mapsto K(\boldsymbol{x},r) \text{ is measurable on } \Gamma_3, \text{ for all } r \in \mathbb{R}_+. \\ \text{(d) The mapping } \boldsymbol{x} \mapsto K(\boldsymbol{x},0) \text{ belongs to } L^2(\Gamma_3). \end{cases} \tag{2.18}$$

$$\begin{cases} \text{(a) } p : \Gamma_3 \times \mathbb{R} \to \mathbb{R}_+. \\ \text{(b) There exists } L_p > 0 \text{ such that } |p(\boldsymbol{x},r_1) - p(\boldsymbol{x},r_2)| \le L_p|r_1-r_2| \\ \qquad \text{for all } r_1,\ r_2 \in \mathbb{R}, \text{ a.e. } \boldsymbol{x} \in \Gamma_3. \\ \text{(c) The mapping } \boldsymbol{x} \mapsto p(\boldsymbol{x},r) \text{ is measurable on } \Gamma_3, \text{ for all } r \in \mathbb{R}. \\ \text{(d) } (p(\boldsymbol{x},r_1) - p(\boldsymbol{x},r_2))(r_1-r_2) \ge 0 \ \ \forall\, r_1,r_2 \in \mathbb{R}, \text{ a.e. } \boldsymbol{x} \in \Gamma_3. \\ \text{(e) } p(\boldsymbol{x},r) = 0 \text{ for all } r \le 0, \text{ a.e. } \boldsymbol{x} \in \Gamma_3. \end{cases} \tag{2.19}$$

For the body forces and tractions densities, we assume

$$\boldsymbol{f}_0 \in C([0,T];L^2(\Omega)^d), \quad \boldsymbol{f}_2 \in C([0,T];L^2(\Gamma_2)^d). \tag{2.20}$$

For the initial data, we assume

$$\boldsymbol{u}_0 \in V, \quad \boldsymbol{\sigma}_0 \in Q. \tag{2.21}$$

Next, we introduce the set of admissible displacements defined by

$$U = \left\{ \boldsymbol{v} \in V : v_\nu \le g \text{ on } \Gamma_3 \right\}. \tag{2.22}$$

Moreover, we define the functions $q : \mathbb{R} \to \mathbb{R}$ and $\boldsymbol{f} : [0,T] \to V$ by the equalities:

$$q(\boldsymbol{x},s) = \int_0^s p(\boldsymbol{x},r)\,\mathrm{d}r \quad \forall\, r \in \mathbb{R}, \text{ a.e. } \boldsymbol{x} \in \Gamma_3, \tag{2.23}$$

$$(\boldsymbol{f}(t),\boldsymbol{v})_V = \int_\Omega \boldsymbol{f}_0(t)\cdot\boldsymbol{v}\,\mathrm{d}x + \int_{\Gamma_2} \boldsymbol{f}_2(t)\cdot\boldsymbol{v}\,\mathrm{d}a \quad \forall\, \boldsymbol{v} \in V,\ t \in [0,T]. \tag{2.24}$$

Assume now that $(\boldsymbol{u}, \boldsymbol{\sigma})$ are sufficiently regular functions which satisfy (2.1)–(2.7), and let $t > 0$ be given. We integrate Eq. (2.1) and make use of the initial conditions (2.7) to obtain

$$\boldsymbol{\sigma}(t) = \mathcal{E}\varepsilon(\boldsymbol{u}(t)) + \int_0^t \mathcal{G}(\boldsymbol{\sigma}(s), \varepsilon(\boldsymbol{u}(s)))\,\mathrm{d}s + \boldsymbol{\sigma}_0 - \mathcal{E}\varepsilon(\boldsymbol{u}_0). \tag{2.25}$$

Then, we use integration by parts, the equilibrium equation (2.2), the boundary conditions (2.3)–(2.6), and notation (2.23), (2.24) to see that

$$(\boldsymbol{\sigma}(t), \varepsilon(\boldsymbol{v}) - \varepsilon(\boldsymbol{u}(t)))_Q + \int_{\Gamma_3} K(\xi(u_\nu)(t))\,(q(v_\nu(t)) - q(u_\nu(t)))\,\mathrm{d}a \geq (\boldsymbol{f}(t), \boldsymbol{v} - \boldsymbol{u}(t))_V \quad \forall\, \boldsymbol{v} \in V. \tag{2.26}$$

Finally, we note that the first inequality in (2.5) combined with the definition (2.22) implies that

$$\boldsymbol{u}(t) \in U. \tag{2.27}$$

We gather (2.25)–(2.27) together to obtain the following variational formulation of Problem $\mathcal{P}$.

Problem $\mathcal{P}_V$ Find a displacement field $\boldsymbol{u} : [0, T] \to U$ and a stress field $\boldsymbol{\sigma} : [0, T] \to Q$ such that

$$\boldsymbol{\sigma}(t) = \mathcal{E}\varepsilon(\boldsymbol{u}(t)) + \int_0^t \mathcal{G}(\boldsymbol{\sigma}(s), \varepsilon(\boldsymbol{u}(s)))\,\mathrm{d}s + \boldsymbol{\sigma}_0 - \mathcal{E}\varepsilon(\boldsymbol{u}_0), \tag{2.28}$$

$$(\boldsymbol{\sigma}(t), \varepsilon(\boldsymbol{v}) - \varepsilon(\boldsymbol{u}(t)))_Q + \int_{\Gamma_3} K(\xi(u_\nu)(t))\,(q(v_\nu(t)) - q(u_\nu(t)))\,\mathrm{d}a \geq (\boldsymbol{f}(t), \boldsymbol{v} - \boldsymbol{u}(t))_V \quad \forall\, \boldsymbol{v} \in U, \tag{2.29}$$

for all $t \in [0, T]$.

The unique solvability of Problem $\mathcal{P}_V$ is given by the following result, proved in [18].

Theorem 2.1 *Assume* (2.16)–(2.21). *Then Problem* $\mathcal{P}_V$ *has a unique solution. Moreover, the solution satisfies*

$$\boldsymbol{u} \in C([0, T]; U), \quad \boldsymbol{\sigma} \in C([0, T]; Q_1). \tag{2.30}$$

We assume in what follows that (2.16)–(2.21) hold, and we denote by $(\boldsymbol{u}, \boldsymbol{\sigma})$ the solution of Problem $\mathcal{P}_V$ stated in Theorem 2.1. For each $\rho > 0$, let K_ρ be a perturbation of the function K which satisfies the condition (2.18) with a positive constant L_{K_ρ}. Consider the following perturbation of Problem $\mathcal{P}_V$.

Problem $\mathcal{P}_V^\rho$ Find a displacement field $\boldsymbol{u}_\rho : [0, T] \to U$ and a stress field $\boldsymbol{\sigma}_\rho : [0, T] \to Q$ such that

$$\boldsymbol{\sigma}_\rho(t) = \mathcal{E}\varepsilon(\boldsymbol{u}_\rho(t)) + \int_0^t \mathcal{G}(\boldsymbol{\sigma}_\rho(s), \varepsilon(\boldsymbol{u}_\rho(s)))\,\mathrm{d}s + \boldsymbol{\sigma}_0 - \mathcal{E}\varepsilon(\boldsymbol{u}_0), \tag{2.31}$$

$$(\boldsymbol{\sigma}_\rho(t), \varepsilon(\boldsymbol{v}) - \varepsilon(\boldsymbol{u}_\rho(t)))_Q + \int_{\Gamma_3} K_\rho(\xi(u_{\rho\nu})(t))\,(q(v_{\rho\nu}(t)) - q(u_{\rho\nu}(t)))\,\mathrm{d}a \geq (\boldsymbol{f}(t), \boldsymbol{v} - \boldsymbol{u}_\rho(t))_V \quad \forall\, \boldsymbol{v} \in U, \tag{2.32}$$

for all $t \in [0, T]$.

It follows from Theorem 2.1 that, for each $\rho > 0$, Problem $\mathcal{P}_V^\rho$ has unique solutions: $(\boldsymbol{u}_\rho, \boldsymbol{\sigma}_\rho)$ and $\boldsymbol{u}_\rho \in C([0, T]; U)$, $\boldsymbol{\sigma}_\rho \in C([0, T]; Q_1)$. In addition, we have the following result, as a consequence of Theorem 5.1 in [18].

Corollary 2.2 *Assume that there exists a function* $G : \mathbb{R}_+ \to \mathbb{R}_+$ *such that*

$$\begin{cases} \text{(a) } |K_\rho(r) - K(r)| \leq G(\rho) \quad \forall\, r \in [0, gT], \text{ for each } \rho > 0. \\ \text{(b) } G(\rho) \to 0 \quad \text{as} \quad \rho \to 0. \end{cases} \tag{2.33}$$

Then the solution $(\boldsymbol{u}_\rho, \boldsymbol{\sigma}_\rho)$ *of Problem* $\mathcal{P}_V^\rho$ *converges to the solution* $(\boldsymbol{u}, \boldsymbol{\sigma})$ *of Problem* $\mathcal{P}_V$*:*

$$\boldsymbol{u}_\rho \to \boldsymbol{u} \quad in \quad C([0,T];V), \quad \boldsymbol{\sigma}_\rho \to \boldsymbol{\sigma} \quad in \quad C([0,T];Q_1) \quad as \quad \rho \to 0. \tag{2.34}$$

Note that Corollary 2.2 states that the weak solution of the viscoplastic contact problem $\mathcal{P}$ depends continuously on the stiffness coefficient.

3 Numerical solution

In this section, we discuss the numerical solution of Problem $\mathcal{P}$. To this end, we use arguments similar to those used in [15,24,25], based on an adapted combination of the penalty method and the augmented Lagrangian method for the numerical treatment of the specific contact condition (2.5). The starting point of our method is an alternative variational formulation of Problem $\mathcal{P}$ by considering a Lagrange multiplier associated with the normal contact stress. Then, an augmented Lagrangian method is naturally used to solve the resulting alternative hybrid variational problem.

3.1 A hybrid variational formulation

In order to derive the hybrid variational problem, we introduce a trace space $X_\nu = \{ v_\nu|_{\Gamma_3} : \boldsymbol{v} \in V\}$. We denote by X_ν' the dual of X_ν and let $\langle \cdot, \cdot \rangle_{X_\nu', X_\nu}$ be the duality pairing. Introduce an operator $\mathcal{K} : X_\nu \to X_\nu'$ and a function $\mathcal{I} : X_\nu \to (-\infty, +\infty]$ by

$$\mathcal{K}\langle u_\nu, v_\nu \rangle_{X_\nu', X_\nu} = \int_{\Gamma_3} K(\xi(u_\nu)) p(u_\nu) v_\nu \, \mathrm{d}a \quad \forall\, u_\nu,\ v_\nu \in X_\nu,$$

$$\mathcal{I}(u_\nu) = \int_{\Gamma_3} I_{\mathbb{R}_-}(u_\nu - g) \, \mathrm{d}a \quad \forall\, u_\nu \in X_\nu,$$

where $I_{\mathbb{R}_-}$ represents the indicator function of the set $\mathbb{R}_- = (-\infty, 0]$.

We note that, for all $t \in (0, T)$, the contact condition (2.5) is equivalent to the subdifferential inclusion:

$$-\sigma_\nu(t) \in \partial \mathcal{I}(u_\nu|_{\Gamma_3}(t)) + \mathcal{K} u_\nu|_{\Gamma_3}(t) \quad \text{in} \quad X_\nu', \tag{3.1}$$

where $\partial \mathcal{I}$ denotes the subdifferential of $\mathcal{I}$ in the sense of the convex analysis. Inclusion (3.1) allows us to supplement the unknowns of the problem with an additional one, the so-called Lagrange multiplier. This leads to the following hybrid variational formulation of the contact problem $\mathcal{P}$.

Problem $\widetilde{\mathcal{P}}_V$ Find a displacement field $\boldsymbol{u} : [0, T] \to V$, a stress field $\boldsymbol{\sigma} : [0, T] \to Q$ and a Lagrange multiplier $\lambda_\nu : [0, T] \to X_\nu'$ such that

$$\boldsymbol{\sigma}(t) = \mathcal{E}\varepsilon(\boldsymbol{u}(t)) + \int_0^t \mathcal{G}(\boldsymbol{\sigma}(s), \varepsilon(\boldsymbol{u}(s))) \, \mathrm{d}s + \boldsymbol{\sigma}_0 - \mathcal{E}\varepsilon(\boldsymbol{u}_0), \tag{3.2}$$

$$(\boldsymbol{\sigma}(t), \varepsilon(\boldsymbol{v}))_Q - \langle \lambda_\nu(t), v_{\nu|_{\Gamma_3}} \rangle_{X_\nu', X_\nu} = (\boldsymbol{f}(t), \boldsymbol{v})_V \quad \forall\, \boldsymbol{v} \in V, \tag{3.3}$$

$$-\lambda_\nu(t) \in \partial \mathcal{I}(u_\nu|_{\Gamma_3}(t)) + \mathcal{K} u_\nu|_{\Gamma_3}(t) \tag{3.4}$$

for all $t \in [0, T]$.

Note that Problem $\widetilde{\mathcal{P}}_V$ represents an alternative to the variational Problem $\mathcal{P}_V$, and is formulated in terms of three unknown fields.

3.2 Numerical approximation

To describe the numerical method for the hybrid variational Problem $\widetilde{\mathcal{P}}_V$, we first introduce some preparatory material. We use a finite element method for the spatial discretization of the domain Ω and a uniform discretization of the time interval $[0, T]$. Assume that Ω is a polyhedral domain, and we denote by $\{\mathcal{T}^h\}$ a regular family of triangular finite element partitions of $\overline{\Omega}$ that are compatible with the boundary decomposition: $\Gamma = \overline{\Gamma_1} \cup \overline{\Gamma_2} \cup \overline{\Gamma_3}$. Here and below, h represents the spatial discretization parameter. In the numerical examples presented in the next section, we approach the space V by the finite dimensional space of continuous piecewise affine functions, denoted V^h. The space Q is approximated by the finite element space of piecewise constants, denoted Q^h. For the discretization of the Lagrange multiplier λ, we consider a discrete space $Y_\nu^h \subset X_\nu' \cap L^2(\Gamma_3)$. For the time discretization, we use evenly spaced nodes $t_n = n\,k$, $0 \le n \le N$, where $N > 0$ is an integer and $k = \frac{T}{N}$ is the time step size. For a continuous function $v(t)$ with values in a function space, we write $v_j = v(t_j)$ for $0 \le j \le N$. Details about the discretization step can be found in [9,26,27].

We now describe the numerical solution of the hybrid variational Problem $\widetilde{\mathcal{P}}_V$. The numerical treatment of the condition (3.4) is based on a combination of the penalty method for the normal compliance contact with an adapted augmented Lagrangian argument for the unilateral condition. To develop the Lagrangian approach, we need to introduce additional fictitious nodes for the Lagrange multiplier in the initial mesh. The introduction of these nodes leads to specific contact elements in relation to the geometrical discretization of the interface Γ_3. For the numerical examples in the next section, we consider a "node-to-rigid" contact element, which is composed of one node of Γ_3 and one Lagrange multiplier node. Details on this construction can be found in [15,24,25,28]. Then, the numerical approximation of Problem $\widetilde{\mathcal{P}}_V$ leads at each time step n to the solution of a system of nonlinear equations of the form:

$$\mathbf{R}(\boldsymbol{u}, \boldsymbol{\lambda}) = \widetilde{\mathbf{G}}(\boldsymbol{u}) + \mathcal{F}(\boldsymbol{u}, \boldsymbol{\lambda}) = \mathbf{0}, \tag{3.5}$$

where the operator $\widetilde{\mathbf{G}}$ comes from the discretization of the elastic terms of the alternative variational Problem $\widetilde{\mathcal{P}}_V$ and the operator $\mathcal{F}$ comes from the discretization of contact terms. In the nonlinear system (3.5), the unknowns are the generalized discrete displacement field $\boldsymbol{u} = \{\boldsymbol{u}^i\}_{i=1}^{N_{\text{tot}}^h} \in \mathbb{R}^{d\cdot N_{\text{tot}}^h}$, and the Lagrange multiplier generalized vector $\boldsymbol{\lambda} = \{\boldsymbol{\lambda}^i\}_{i=1}^{N_{\Gamma_3}^h} \in \mathbb{R}^{d\cdot N_{\Gamma_3}^h}$ in which N_{tot}^h and $N_{\Gamma_3}^h$ are the total number of nodes issued from the discretization of Ω and Γ_3, respectively. Here $\boldsymbol{u}^i$ represents the value of the function $\boldsymbol{u}^h$ at the i-th node of $\mathcal{T}^h$, and $\boldsymbol{\lambda}^i$ denotes the value of the function $\boldsymbol{\lambda}^h$ at the i-th node of the discretized contact interface. In addition, $\widetilde{\mathbf{G}}(\boldsymbol{u}) \in \mathbb{R}^{d\cdot N_{\text{tot}}^h} \times \mathbb{R}^{d\cdot N_{\Gamma_3}^h}$ represents the generalized elastic term and is defined by $\widetilde{\mathbf{G}}(\boldsymbol{u}) = (\mathbf{G}(\boldsymbol{u}), \mathbf{0}_{d\cdot N_{\Gamma_3}^h})$, where $\mathbf{0}_{d\cdot N_{\Gamma_3}^h}$ is the zero element of $\mathbb{R}^{d\cdot N_{\Gamma_3}^h}$ and the term $\mathbf{G}(\boldsymbol{u}) \in \mathbb{R}^{d\cdot N_{\text{tot}}^h}$ is given by the equality:

$$(\mathbf{G}(\boldsymbol{u}) \cdot \boldsymbol{v})_{\mathbb{R}^{d\times N_{\text{tot}}^h}} = (\boldsymbol{\sigma}^h, \varepsilon(\boldsymbol{v}^h))_Q - (\boldsymbol{f}, \boldsymbol{v}^h)_V \quad \forall\, \boldsymbol{v} = \{\boldsymbol{v}^i\}_{i=1}^{N_{\text{tot}}^h}, \quad \forall\, \boldsymbol{v}^h \in V^h,$$

where $\boldsymbol{\sigma}^h$ is related to $\boldsymbol{u}^h$ by the discrete constitutive law (3.2). The contact operator $\mathcal{F}(\boldsymbol{u}, \boldsymbol{\lambda})$ in equation (3.5) is related to the contact condition, (3.4). It is defined by

$$\begin{aligned}(\mathcal{F}(\boldsymbol{u}, \boldsymbol{\lambda}) \cdot (\boldsymbol{v}, \boldsymbol{\gamma}))_{\mathbb{R}^{d\cdot N_{\text{tot}}^h} \times \mathbb{R}^{d\cdot N_{\Gamma_3}^h}} &= \int_{\Gamma_3} \Big((\lambda_\nu^h + r(u_\nu^h - g))_+ \boldsymbol{\nu} \Big) \cdot \boldsymbol{v}^h \, \mathrm{d}a \\ &+ \int_{\Gamma_3} \frac{-1}{r} \Big(\boldsymbol{\lambda}^h - (\lambda_\nu^h + r(u_\nu^h - g))_+ \boldsymbol{\nu} \Big) \cdot \boldsymbol{\gamma}^h \, \mathrm{d}a \\ &+ \int_{\Gamma_3} K(\xi(\chi_{[0,g]}(u_\nu^h) u_\nu^h) p(\chi_{[0,g]}(u_\nu^h) u_\nu^h) \boldsymbol{\nu} \cdot \boldsymbol{v}^h \mathrm{d}a\end{aligned}$$

for $\boldsymbol{u}, \boldsymbol{v} \in \mathbb{R}^{d\cdot N_{\text{tot}}^h}$, $\boldsymbol{\lambda}, \boldsymbol{\gamma} \in \mathbb{R}^{d\cdot N_{\Gamma_3}^h}$, $\boldsymbol{u}^h, \boldsymbol{v}^h \in V^h$, and $\boldsymbol{\lambda}^h, \boldsymbol{\gamma}^h \in Y_\nu^h$, where r is a positive penalty coefficient, and χ_E represents the characteristic function of the set E. In contrast to the problem studied in [15], here we have

to consider the discretization of the history-dependent term $\xi(\chi_{[0,g]}(u_\nu^h)u_\nu^h)$ and, to this end, we used an implicit rectangular method by approximating $\xi(r)(t_n)$ with $\sum_{i=1}^{n} k\,(r_+)_i$.

The nonlinear system (3.5) is solved by a generalized Newton method. The pair $\tilde{\boldsymbol{u}} = (\boldsymbol{u}, \boldsymbol{\lambda})$ is computed simultaneously by using the following linearized iterative scheme:

$$\begin{aligned}
&\text{For } i = 0, \ldots, \\
&\text{Solve } (\mathbf{K}_i + \mathbf{T}_i)\Delta\tilde{\boldsymbol{u}}_{i+1} = -\mathbf{R}(\tilde{\boldsymbol{u}}_i) \\
&\tilde{\boldsymbol{u}}_{i+1} = \tilde{\boldsymbol{u}}_i + \Delta\tilde{\boldsymbol{u}}_{i+1}, \\
&\text{until convergence.}
\end{aligned} \tag{3.6}$$

At each Newton iteration of index i, the linear symmetric system (3.7) is solved by using a conjugate gradient method with efficient preconditioners, in order to overcome the poor conditioning of the system matrix due to the contact terms. For instance, we use an ILU preconditioner based on an Element-By-Element procedure, see [29] for details. The coefficient matrix of the linear system (3.7) is the sum of an elastic stiffness matrix $\mathbf{K}_i$ and a contact tangent matrix $\mathbf{T}_i$. Note that $\mathbf{K}_i = D_{\tilde{\boldsymbol{u}}}\mathbf{G}(\boldsymbol{u})$ represents the differential of the functions $\mathbf{G}$ with respect to the variable $\tilde{\boldsymbol{u}}$, and $\mathbf{T}_i \in \partial_{\tilde{\boldsymbol{u}}}\mathcal{F}(\tilde{\boldsymbol{u}}_i)$ represents the generalized Jacobian of $\mathcal{F}$ at $\tilde{\boldsymbol{u}}_i$. Due to the fact that the measure of the set of the points in which the function $\mathcal{F}$ is nondifferentiable is zero, $\mathbf{T}_i$ is reduced to a single-valued classical Jacobian matrix. In the case of the "node-to-rigid" contact element composed of one elastic node of Γ_3 and one contact Lagrange multiplier node, the elementary contact tangent matrix $\mathbf{T}_i^{ec}$ takes the form:

$$\mathbf{T}_i^{ec} = \begin{pmatrix} r(\boldsymbol{M}+\boldsymbol{N}) & \boldsymbol{M} \\ \boldsymbol{M} & \frac{1}{r}(\boldsymbol{M}-\boldsymbol{I}) \end{pmatrix}.$$

Here $\boldsymbol{I}$ is the 2×2 identity matrix, $\boldsymbol{N}$ and $\boldsymbol{M}$ are 2×2 block matrices which are defined according to the contact state:

$$\boldsymbol{N} = \begin{cases} \mathbf{0} & \text{if } u_\nu < 0, \\ u_\nu^+ \boldsymbol{v}\otimes D_{\mathbf{u}}K(\xi) + K(\xi)\boldsymbol{v}\otimes\boldsymbol{v} & \text{if } 0 \le u_\nu < g, \end{cases}$$

and

$$\boldsymbol{M} = \begin{cases} \mathbf{0} & \text{if } u_\nu < g, \\ \boldsymbol{v}\otimes\boldsymbol{v} & \text{if } u_\nu \ge g, \end{cases}$$

where $\mathbf{0}$ is the 2×2 zero matrix, and $\boldsymbol{u}\otimes\boldsymbol{v}$ represents the tensor product of two vectors $\boldsymbol{u}$ and $\boldsymbol{v}$, defined by $(\boldsymbol{u}\otimes\boldsymbol{v})_{l,m} = u_l v_m$ in which $l, m = 1, \ldots, d$. The global contact tangent matrix $\mathbf{T}_i$ is obtained by a finite element assembly procedure from all the contact elements $\mathbf{T}_i^j$, $1 \le j \le N_{\Gamma_3}^h$.

4 Numerical simulations

The aim of this section is to present some results of numerical simulations. We pay particular attention to the mechanical interpretation of the contact condition (2.5). We complete them with two parametric studies which illustrate the dependence of the numerical solution with respect to the stiffness coefficient and the numerical discretization parameters.

4.1 The physical setting

A representative academic example of compression of a ball against a foundation is considered. Due to the symmetry of the problem, we only need to consider the physical setting depicted in Fig. 1. There,

$$\Omega = \left\{(x_1, x_2) \in \mathbb{R}^2 :\ x_1 > 0,\ x_1^2 + (x_2 - 1)^2 < 1\right\},$$

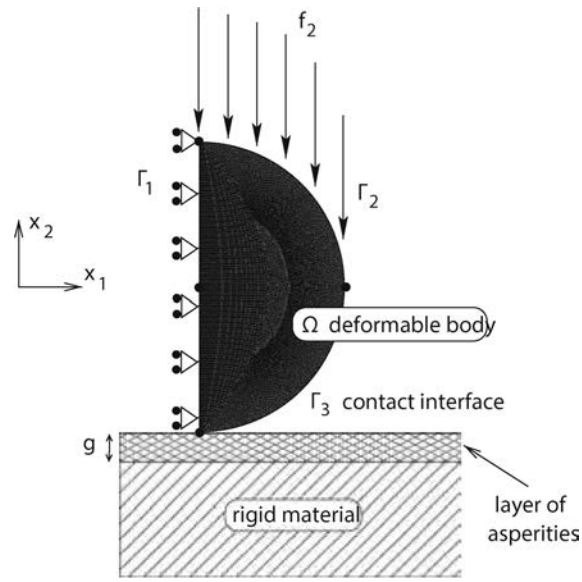

Fig. 1 Physical setting: compression of a half-ball against a foundation

$$\Gamma_1 = \{0\} \times [0, 2],$$
$$\Gamma_2 = \left\{(x_1, x_2) \in \mathbb{R}^2 : \ x_1 \geq 0, \ x_2 \geq 1, \ x_1^2 + (x_2 - 1)^2 = 1\right\},$$
$$\Gamma_3 = \left\{(x_1, x_2) \in \mathbb{R}^2 : \ x_1 \geq 0, \ x_2 < 1, \ x_1^2 + (x_2 - 1)^2 = 1\right\}.$$

The domain Ω represents the cross section of a three-dimensional deformable body subject to the action of tractions in such a way that a plane stress hypothesis is valid. The horizontal component of the displacement field vanishes on Γ_1 and vertical tractions act on Γ_2. No body forces are assumed to act on the body during the process. The body is in frictionless contact with an obstacle on the part Γ_3 of its boundary. For the discretization in Fig. 1, we use 30,808 elements with 128 elements containing sides on the contact boundary.

We assume that the mechanical response of the ball is purely elastic, i.e., we model the material's behavior with a constitutive law of the form (1.1) in which the function $\mathcal{G}$ vanishes. In addition, we assume that the material is homogeneous and isotropic. We denote by E and κ the Young modulus and the Poisson ratio of the material, respectively, and use δ_{ij} for the Kronecker symbol. Then, the elasticity tensor $\mathcal{E}$ is given by

$$(\mathcal{E}\boldsymbol{\tau})_{ij} = \frac{E\kappa}{(1+\kappa)(1-2\kappa)}(\tau_{ii})\delta_{ij} + \frac{E}{1+\kappa}\tau_{ij}, \qquad 1 \leq i, j \leq 2, \tag{4.1}$$

where the summation convention is used. For the numerical experiments, we use the following data:

$$E = 1000\,\mathrm{N/m^2}, \quad \kappa = 0.3,$$
$$\boldsymbol{f}_0 = (0, 0)\,\mathrm{N/m^2}, \quad \boldsymbol{f}_2 = (-1000 \times t, 0)\,\mathrm{N/m} \quad \text{on } \Gamma_2,$$
$$p(r) = r_+, \quad K(\xi) = c_v(1 + \alpha\xi)^\beta \ \text{ where } \ \xi(r)(t_n) = \sum_{i=0}^{n} k\,(r_+)_i,$$
$$c_v = 100\,\mathrm{N/m^2}, \quad \alpha = 20, \quad \beta = \pm 1, \quad g = 0.2\,\mathrm{m},$$
$$T = 1.1\,\mathrm{s}, \quad N = 11, \quad k = 0.1.$$

We note that for $\beta = 1$ the function $\xi \mapsto K(\xi)$ is increasing and, therefore, the stiffness coefficient increases with the history of the penetration. This behavior models the hardening process of the foundation. In contrast, for $\beta = -1$, the function $\xi \mapsto K(\xi)$ is decreasing, and, therefore, the stiffness coefficient decreases with the history of the penetration. This behavior models the softening process of the foundation.

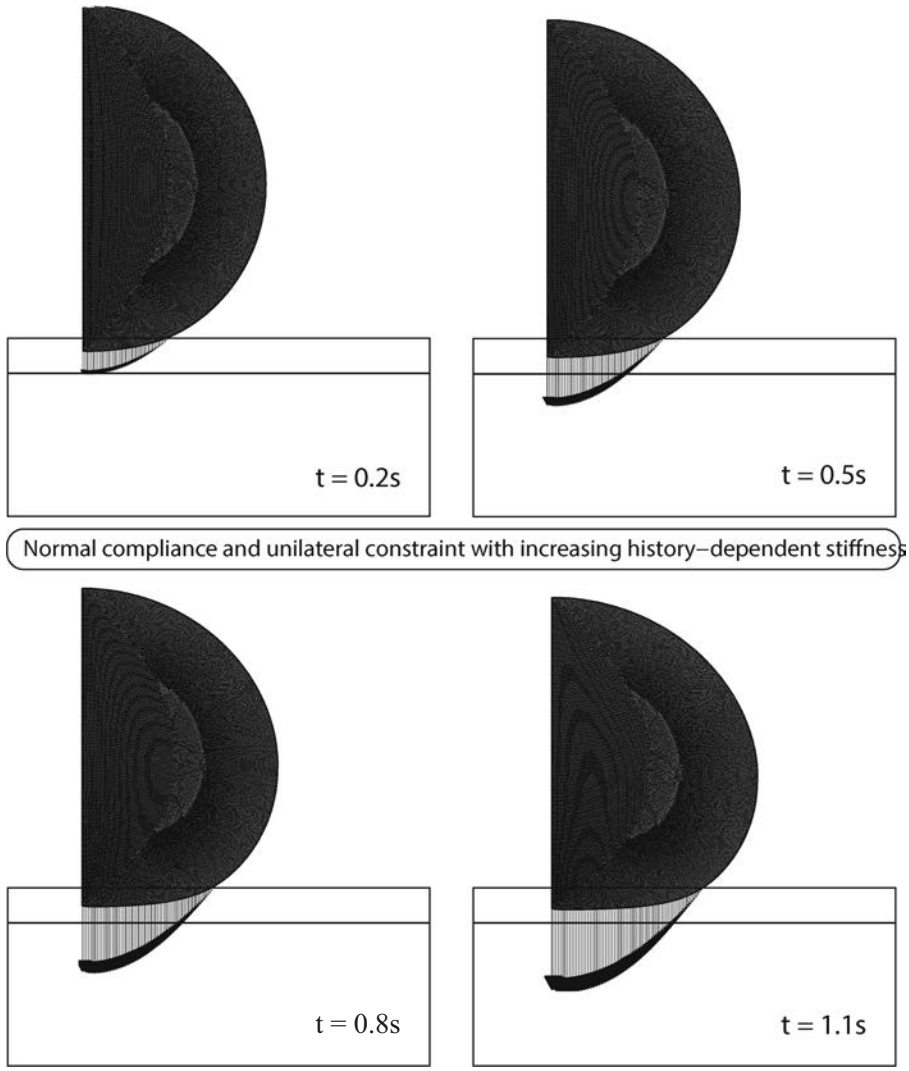

Fig. 2 Evolution of deformed meshes and contact interfaces forces in the case $\beta = 1$

4.2 Mechanical interpretation of the contact model

Our numerical simulation results are depicted in Figs. 2–7. Below we provide some comments on these results, with emphasis on their mechanical interpretations.

First, in Fig. 2, we show the deformed meshes and the contact interface forces with $\beta = 1$, at times $t = 0.2\,\mathrm{s}$, $t = 0.5\,\mathrm{s}$, $t = 0.8\,\mathrm{s}$ and $t = 1.1\,\mathrm{s}$. In Fig. 3, we show the deformed meshes and the contact interface forces at the same moments of time, in the case where $\beta = -1$. A comparison of these figures reveals that, at each time moment, the penetrations obtained with $\beta = 1$ are smaller than that with $\beta = -1$. This agrees with the fact that the case $\beta = 1$ corresponds to a hardening of the layer of thickness g whereas $\beta = -1$ corresponds to a softening of the layer.

Note that in Fig. 2, all the contact nodes are in the state of normal compliance, since the penetration does not reach the limit g. In contrast, in Fig. 3, a large proportion of the contact nodes is in the state of unilateral contact; there, the complete flattening of the asperities of size $g = 0.2\,\mathrm{m}$ is reached, due to the decreasing of the stiffness coefficient. This behavior is confirmed in Fig. 4 in which the evolution of the stiffness coefficient is plotted at

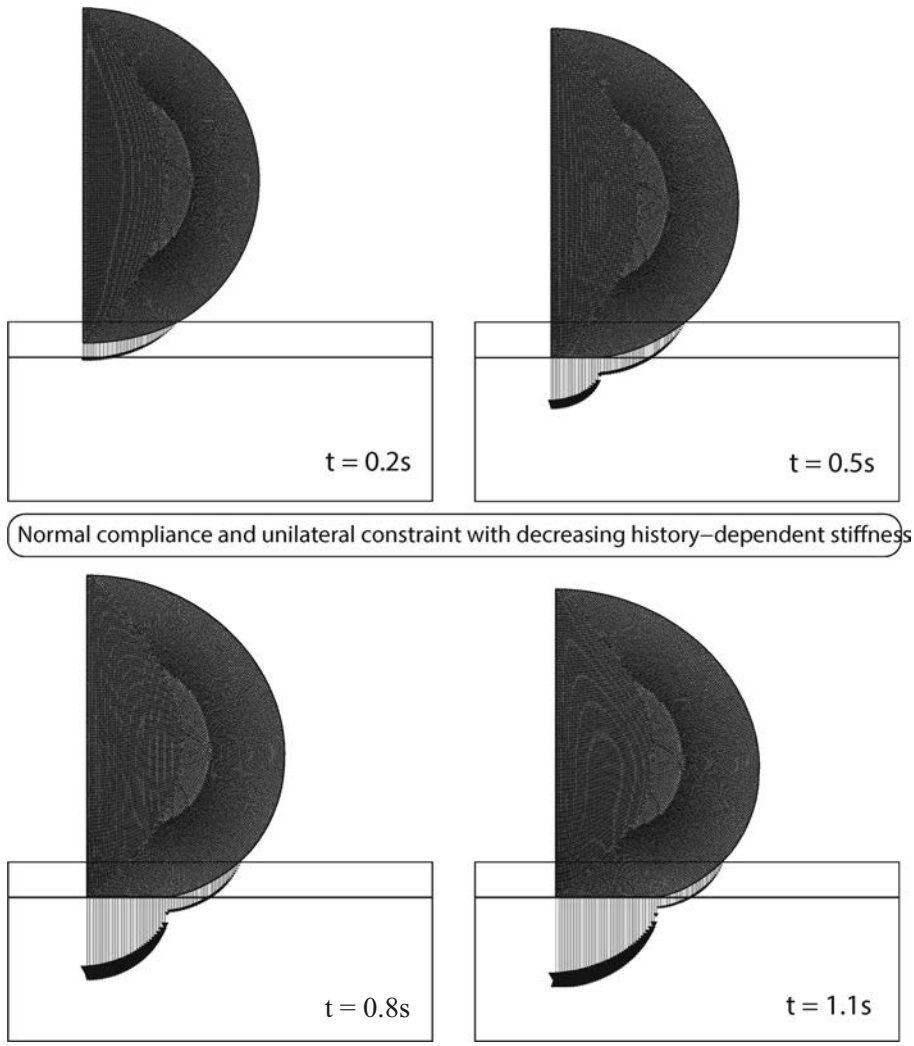

Fig. 3 Evolution of deformed meshes and contact interfaces forces in the case $\beta = -1$

each time increment of the process, for both cases of history dependence. We note that the coefficient grows from $100\,\mathrm{N/m^2}$ to $323\,\mathrm{N/m^2}$ for the case $\beta = 1$, while the coefficient decreases from $100\,\mathrm{N/m^2}$ to $21\,\mathrm{N/m^2}$ for the case $\beta = -1$.

We now compare the contact condition (2.5) with two other contact conditions, found in the literature, which can be obtained as limit cases of (2.5). The first one is a contact condition with normal compliance and unilateral constraint, introduced in [13] and studied in [15,16]; it can be obtained from the condition (2.5) in the case where K is a constant, and it models the contact with an elastic-rigid foundation, without hardening or softening. The second one is the classical normal compliance condition introduced in [22] and studied, for instance, in [19–21]; this condition models the contact with an elastic foundation; it is characterized by the fact that the penetrations are not limited, and it can be obtained from the contact condition (2.5) in the limit $g \to \infty$.

To perform our comparison, in the upper two graphs in Fig. 5, we plot the deformed configurations as well as the contact interface forces corresponding to Problem $\mathcal{P}_V$ at the final time $t = 1.1\,\mathrm{s}$, in the case $\beta = 1$ and $\beta = -1$. In the lower two graphs, we plot the deformed configurations as well as the contact interface forces corresponding

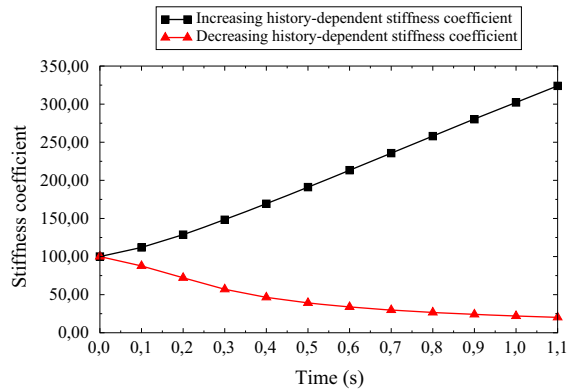

Fig. 4 Evolution of the history-dependent stiffness coefficient during the time process

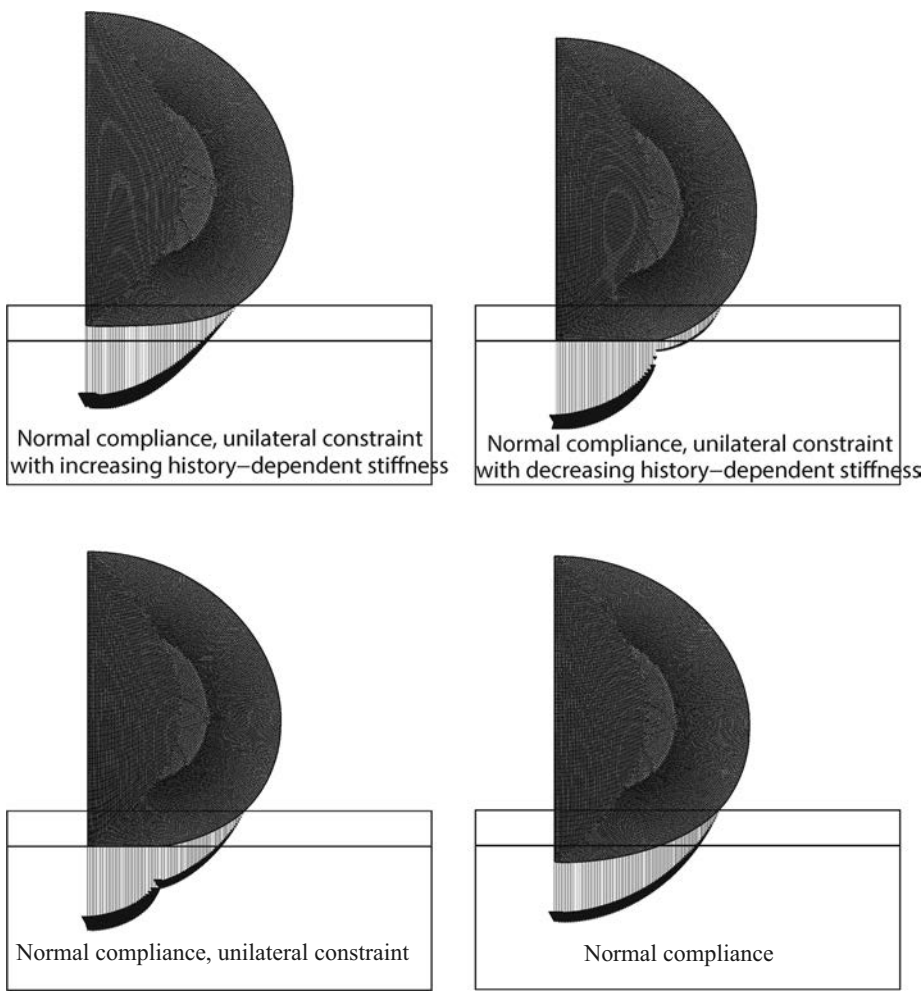

Fig. 5 Deformed mesh and contact interface forces for Problem $\mathcal{P}_V$ at $t = 1.1\,\mathrm{s}$ for various cases of the contact condition (2.5)

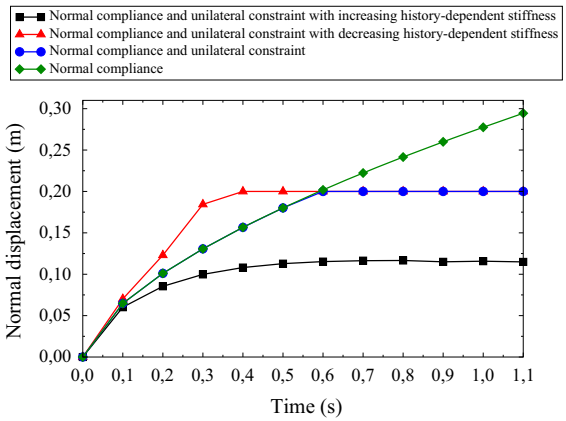

Fig. 6 Evolution of the penetration for various cases of contact conditions during the time process

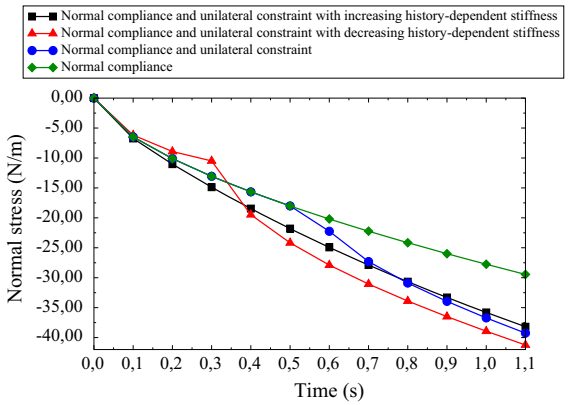

Fig. 7 Evolution of the normal contact stress for various cases of contact conditions during the time process

to Problem $\mathcal{P}_V$ with $\alpha = 0$, $g = 0.2\,\mathrm{m}$ and $\alpha = 0$, $g = 2000\,\mathrm{m}$, respectively, which correspond to the contact condition with normal compliance and unilateral constraint and the classical normal compliance contact condition, respectively. Observe that the penetrations obtained in the case with increasing stiffness coefficient (the case $\beta = 1$) are smaller than the penetrations obtained in the case where the stiffness coefficient is constant (the case of normal compliance with unilateral constraint and the case of normal compliance). The penetrations obtained in the case with decreasing stiffness coefficient (the case $\beta = -1$) are larger than that obtained in the case where the stiffness coefficient is constant (the case of normal compliance with unilateral constraint and the case of normal compliance). This behavior is, again, a consequence of the hardness and softness of the foundation. It is confirmed in Fig. 6, where the penetrations and the normal contact stresses are plotted at each time increment of the process. The magnitude of the corresponding normal stresses related these four cases of contact conditions, at each time increment of the process, is plotted in Fig. 7.

4.3 Parametric studies

We now proceed with two parametric studies which highlight the behavior of the numerical solution of the contact problem with respect to the stiffness coefficient, on one hand, and illustrate the numerical convergence of the discrete scheme, on the other hand.

First, we present numerical evidence of the convergence result given in Corollary 2.2. To this end, we consider the discrete solution $(\boldsymbol{u}_\rho^{hk}, \boldsymbol{\sigma}_\rho^{hk})$ of the perturbated Problem $\mathcal{P}_V^\rho$ constructed with the perturbed stiffness coefficient $K_\rho(\xi) = \rho c_v (1+\alpha\xi)^\beta$, with ρ being a small positive parameter which converges to zero. We denote by $(\boldsymbol{u}_*^{hk}, \boldsymbol{\sigma}_*^{hk})$ the discrete solution of the contact Problem $\mathcal{P}_V$ with $K \equiv 0$. Obviously, the functions K_ρ and $K \equiv 0$ satisfy condition (2.33); therefore, Corollary 2.2 applies. Also, note that for $K \equiv 0$, the contact conditions (2.5) reduce to the classical Signorini condition in a form with the gap g, which models the contact with a perfectly rigid foundation. We denote by $\mathcal{P}_V^*$ this particular form of Problem $\mathcal{P}$ and stress that it describes a limit situation when the layer of soft materials disintegrates by itself and does not offer resistance to penetration.

In Fig. 8, we plot the numerical estimations of the following difference:

$$\|\boldsymbol{u}_\rho^{hk} - \boldsymbol{u}_*^{hk}\|_V + \|\boldsymbol{\sigma}_\rho^{hk} - \boldsymbol{\sigma}_*^{hk}\|_Q$$

at the time $t = 1.1\,\mathrm{s}$, for various values of the parameter ρ. We change ρ from 1 to 10^{-6}. We note that these numerical estimations converge to zero when ρ tends to zero. This provides numerical evidence of the convergence

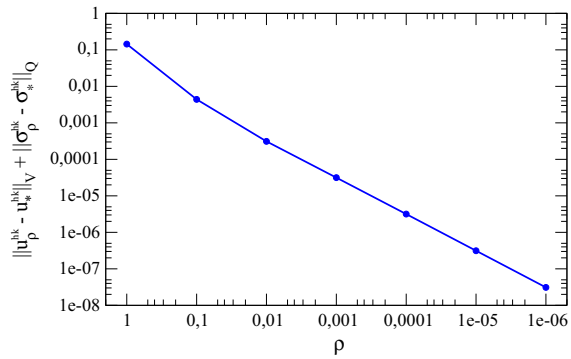

Fig. 8 Numerical estimates of at $t = 1.1$ s for various values of the parameter ρ

result (2.34). This convergence is also illustrated in Fig. 9, in which we plot the deformed configurations as well as the contact interface forces for four values of the parameter ρ. We note that for $\rho = 1$, all the contact nodes are in the state of normal compliance, while for $\rho = 0.01$, almost all the contact nodes are in the state of unilateral contact with a gap $g = 0.2$ m.

Finally, we provide a parametric study with respect to the discretization parameters h and k in order to investigate the numerical convergence order of the fully discrete scheme. To this end, we compute a sequence of numerical solutions obtained by using uniform partitions of the time interval $[0, T]$ and quasi-uniform triangulations of the domain Ω. We start with the values $h = 1/4$ and $k = 1/4$ which are successively halved. The parameter h represents the average size of a finite element of the mesh, and k is the time step. The numerical results reported in Figs. 1, 2, 3, 4, 5, 6, and 7 correspond to $h = 1/128$ and $k = 1/128$. In addition, the numerical solution for $h = 1/512$ and $k = 1/512$ is taken as the "true" solution $\boldsymbol{u}$, and we presume that this discretization corresponds to a problem with 472,074 degrees of freedom and 470,252 elements. Then, we compute the numerical errors $\|\boldsymbol{u} - \boldsymbol{u}^{hk}\|_V$ at $t = 1.1s$ for several values of the discretization parameters h and k. The numerical results are presented in Fig. 10, where the dependence of the error estimates on the sum $h + k$ is plotted. We conclude from here that our numerical method has a linear asymptotical convergence behavior with respect to the discretization parameters h and k. A rigorous proof of this statement represents an open question which, clearly, deserves to be investigated in the future.

5 Discussion

Studies of contact problems related to modeling, mathematical analysis, numerical analysis, and numerical simulations have attracted steady attention from researchers in engineering and mathematics. This paper provides a numerical study of a newly formulated model in contact mechanics. The model concerns frictionless contact for viscoplastic materials. The process is quasistatic, and the contact is modeled with normal compliance and unilateral constraint; the novelty of the model is due to the fact that the stiffness coefficient is allowed to depend on the history of the penetration. The problem is highly nonlinear, and it is represented by a system of nonlinear, multivalued equations. The main contribution of the paper is the introduction of an efficient numerical method to solve the problem. Numerical results on some examples are reported to show the good performance of the method.

Further work along the lines of the subject of the paper are (a) a rigorous error analysis of the numerical method, including convergence and error estimates; and (b) adaptive solution algorithms. These tasks are by no means trivial, due to the form of the boundary integral term in the variational inequality of the system. To develop adaptive solution algorithms, it is necessary to first derive a posteriori error estimate for the numerical method (cf. [30–36] on a posteriori error analysis and adaptive solution algorithms for simpler models of elliptic or parabolic variational inequalities). Success of the work on these two aspects will not only lead to more efficient and effective numerical methods for solving the contact problem of this paper, but also be useful in numerically solving other history-dependent contact problems.

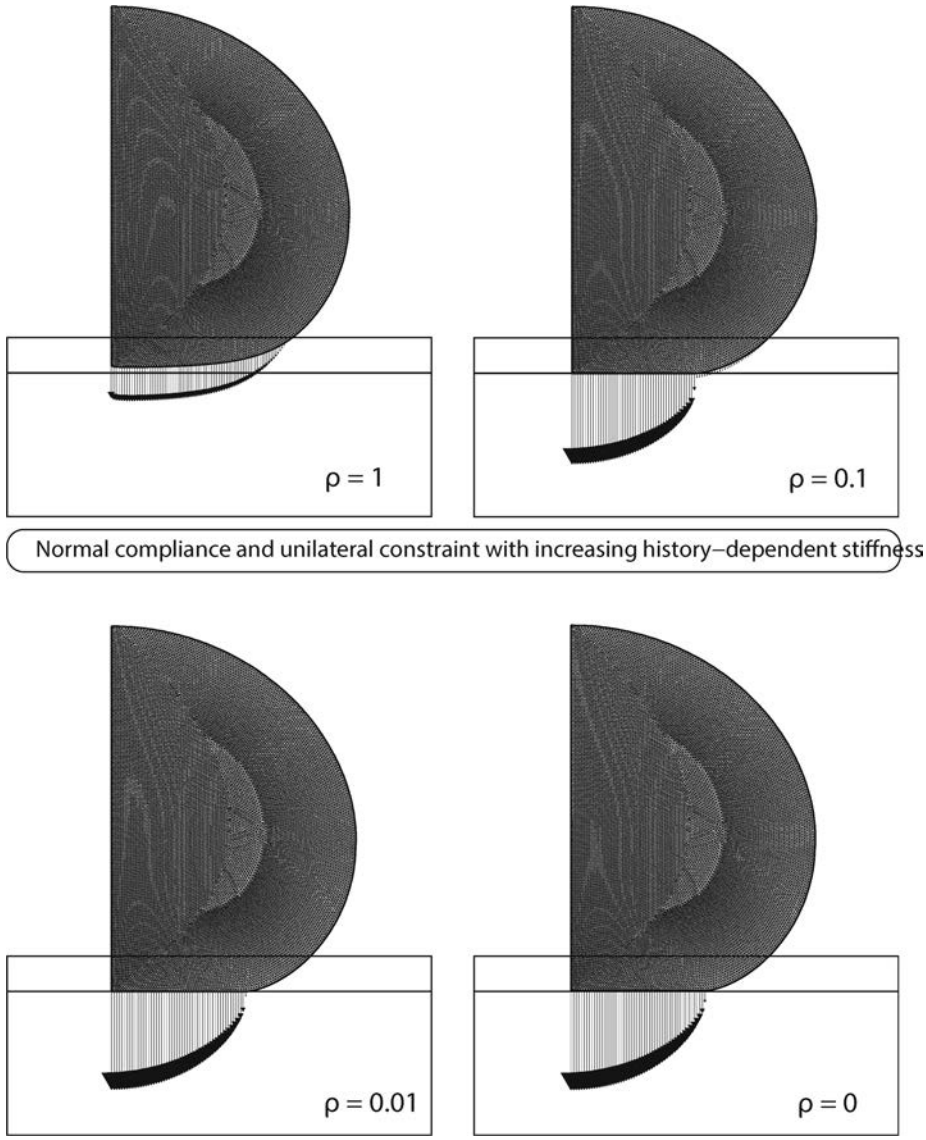

Fig. 9 Deformed mesh and contact interface forces for Problem $\mathcal{P}_V^\rho$ at $t = 1.1\,\mathrm{s}$, for various parameters of ρ

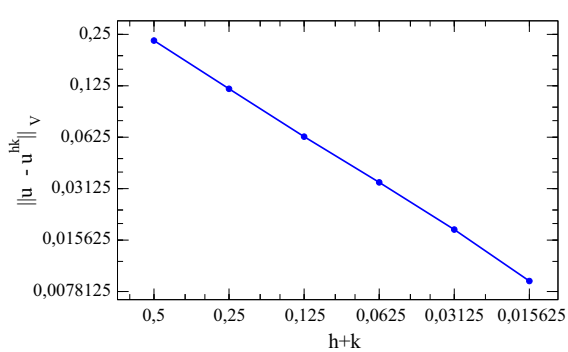

Fig. 10 Numerical error estimates at $t = 1.1\,\mathrm{s}$

Acknowledgments This work was supported by a the Marie Curie International Research Staff Exchange Scheme Fellowship within the 7th European Community Framework Programme under Grant Agreement No. 295118. The work of the second author was also supported by grants from the Simons Foundation.

References

1. Eck C, Jarušek J, Krbeč M (2005) Unilateral Contact problems: variational methods and existence theorems. Pure and applied mathematics, vol 270. Chapman/CRC Press, New York
2. Han W, Sofonea M (2002) Quasistatic contact problems in viscoelasticity and viscoplasticity. Studies in advanced mathematics, vol 30. American Mathematical Society-International Press, Baltimore
3. Panagiotopoulos PD (1985) Inequality problems in mechanics and applications. Birkhäuser, Boston
4. Shillor M, Sofonea M, Telega J (2004) Models and variational analysis of quasistatic contact. Lecture notes in physics, vol 655. Springer, Berlin
5. Haslinger J, Hlavácek I, Nečas J (1996) Numerical methods for unilateral problems in solid mechanics. In: Lions J-L, Ciarlet P (eds) Handbook of numerical analysis, vol IV. North-Holland, Amsterdam, pp 313–485
6. Hlaváček I, Haslinger J, Nečas J, Lovíšek J (1988) Solution of variational inequalities in mechanics. Springer-Verlag, New York
7. Kikuchi N, Oden JT (1988) Contact problems in elasticity: a study of variational inequalities and finite element methods. SIAM, Philadelphia
8. Laursen T (2002) Computational contact and impact mechanics. Springer, Berlin
9. Wriggers P (2002) Computational contact mechanics. Wiley, Chichester
10. Migórski S, Shillor M, Sofonea M (eds) (2015) Special issue on contact mechanics. Nonlinear Anal 22:435–679
11. Cristescu N, Suliciu I (1982) Viscoplasticity. Martinus Nijhoff Publishers, Editura Tehnica, Bucharest
12. Ionescu IR, Sofonea M (1993) Functional and numerical methods in viscoplasticity. Oxford University Press, Oxford
13. Jarušek J, Sofonea M (2008) On the solvability of dynamic elastic-visco-plastic contact problems. Zeitschrift für Angewandte Matematik und Mechanik (ZAMM) 88:3–22
14. Sofonea M, Matei A (2012) Mathematical models in contact mechanics. London Mathematical Society lecture note series, vol 398. Cambridge University Press, Cambridge
15. Barboteu M, Matei A, Sofonea M (2012) Analysis of quasistatic viscoplastic contact problems with normal compliance. Quart J Mech Appl Math 65:555–579
16. Barboteu M, Matei A, Sofonea M (2014) On the behaviour of the solution of a viscoplastic contact problem. Quart Appl Math 72:625–647
17. Sofonea M, Matei A (2004) A mixed variational formulation for the Signorini frictionless problem in viscoplasticity. Ann Univ Ovidius Constanta 12:157–170
18. Sofonea M, Shillor M (2014) A viscoplastic contact model with normal compliance, unilateral constraint and history-dependent stiffness coefficient. Commun Pure Appl Anal 13:371–387
19. Klarbring A, Mikelič A, Shillor M (1988) Frictional contact problems with normal compliance. Int J Eng Sci 26:811–832
20. Klarbring A, Mikelič A, Shillor M (1989) On friction problems with normal compliance. Nonlinear Anal 13:935–955
21. Martins JAC, Oden JT (1987) Existence and uniqueness results for dynamic contact problems with nonlinear normal and friction interface laws. Nonlinear Anal 11:407–428
22. Oden JT, Martins JAC (1985) Models and computational methods for dynamic friction phenomena. Comput Methods Appl Mech Eng 52:527–634
23. Piotrowski J (2010) Smoothing dry friction damping by dither generated in rolling contact of wheel and rail and its influence on ride dynamics of freight wagons. Veh Syst Dyn 48:675–703
24. Barboteu M, Cheng X-L, Sofonea M (2014) Analysis of a contact problem with unilateral constraint and slip-dependent friction. Math Mech Solids. doi:10.1177/1081286514537289
25. Barboteu M, Bartosz K, Kalita P, Ramadan A (2014) Analysis of a contact problem with normal compliance, finite penetration and nonmonotone slip dependent friction. Commun Contemp Math 16(1):1350016
26. Khenous HB, Pommier J, Renard Y (2006) Hybrid discretization of the Signorini problem with Coulomb friction. Theoretical aspects and comparison of some numerical solvers. Appl Numer Math 56:163–192
27. Khenous HB, Laborde P, Renard Y (2006) On the discretization of contact problems in elastodynamics. Lect Notes Appl Comput Mech 27:31–38
28. Alart P, Curnier A (1991) A mixed formulation for frictional contact problems prone to Newton like solution methods. Comput Methods Appl Mech Eng 92:353–375
29. Alart P, Barboteu M, Lebon F (1997) Solutions of frictional contact problems using an *EBE* preconditioner. Comput Mech 30:370–379
30. Bartels S, Carstensen C (2004) Averaging techniques yield reliable a posteriori finite element error control for obstacle problems. Numer Math 99:225–249
31. Bostan V, Han W (2004) Recovery-based error estimation and adaptive solution of elliptic variational inequalities of the second kind. Commun Math Sci 2:1–18

32. Bostan V, Han W (2006) A posteriori error analysis for a contact problem with friction. Comput Methods Appl Mech Eng 195:1252–1274
33. Bostan V, Han W, Reddy BD (2005) A posteriori error estimation and adaptive solution of elliptic variational inequalities of the second kind. Appl Numer Math 52:13–38
34. Han W (2005) A posteriori error analysis via duality theory, with applications in modeling and numerical approximations. Springer, New York
35. Moon K-S, Nochetto RH, von Petersdorff T, Zhang C (2007) A posteriori error analysis for parabolic variational inequalities, M2AN Math. Mode. Numer Anal 41:485–511
36. Nochetto RH, Siebert KG, Veeser A (2003) Andreas, Pointwise a posteriori error control for elliptic obstacle problems. Numer Math 95:163–195